www.sciencemag.org/cgi/content/full/science.1237515/DC1

Supplementary Materials for

Inhibition of RNA Helicase Brr2 by the C-Terminal Tail of the Spliceosomal Protein Prp8

Sina Mozaffari-Jovin, Traudy Wandersleben, Karine F. Santos, Cindy L. Will, Reinhard Lührmann,* Markus C. Wahl*

*Corresponding author. E-mail: reinhard.luehrmann@mpi-bpc.mpg.de (R.L.); mwahl@zedat.fu-berlin.de (M.C.W.)

Published 23 May 2013 on *Science* Express
DOI: 10.1126/science.1237515

This PDF file includes:

Materials and Methods
Figs. S1 to S10
Tables S1 and S2
References (*22*–*31*)

Materials and Methods

Production and analysis of recombinant human proteins

Human proteins were used for crystallographic analyses and for interaction studies (fig. S2) and activity assays (fig. S6) that involved the isolated Brr2 N-terminal cassette, as the N-terminal cassette of yeast Brr2 could not be produced in soluble form. A DNA fragment encoding hPrp8^{Jab1} (residues 2064-2335) was PCR-amplified using a synthetic gene encoding hPrp8 as a template and cloned into the BamHI and XhoI sites of pGEX-6P-1 (GE Healthcare). The GST-hPrp8^{Jab1}-encoding region was subcloned into EcoRI and HindIII sites of a pFL vector (*22*). An expression construct for hPrp8$^{Jab1\text{-}\Delta C15}$ was obtained by introduction of a stop codon *via* the QuikChange protocol (Stratagene). All proteins were produced in insect cells as described previously (*18*).

For purification of hPrp8^{Jab1}, the cell pellet was resuspended in 50 mM Tris-HCl, pH 8.0, 300 mM NaCl, 1 mM DTT, 5 % glycerol, 0.05 % NP-40, supplemented with protease inhibitors (Roche) and DNase I. Cells were lyzed by sonication using a Sonopuls Ultrasonic Homogenizer HD 3100 (Bandelin) and centrifuged for 1h at 53000 x g. The cleared lysate was loaded onto a Glutathione-Sepharose 4B resin (GE Healthcare) equilibrated with buffer A (50 mM Tris-HCl, pH 8.0, 300 mM NaCl, 1 mM DTT, 5% glycerol), incubated for 1h and eluted with buffer A plus 10 mM reduced glutathione. The sample was buffer-exchanged using a HiPrep 26/60 desalting column (GE Healthcare) equilibrated with buffer A and the GST-hPrp8^{Jab1} fragment was cleaved overnight at 4°C with PreScission protease. The cleaved protein was loaded again on the affinity resin to remove uncleaved protein, GST and the protease. The flow-through was combined with purified hBrr2^{HR} in a 2:1 (hPrp8^{Jab1}:hBrr2^{HR}) molar ratio. The hBrr2^{HR}-hPrp8^{Jab1} complex was further purified by gel filtration on a 16/60 Superdex 200 column (GE Healthcare) in 20 mM Tris-HCl, pH 8.0, 150 mM NaCl, 1 mM DTT. hPrp8$^{Jab1\text{-}\Delta C15}$ and hBrr2^{HR}-hPrp8$^{Jab1\text{-}\Delta C15}$ complex were obtained in the same fashion.

hBrr2^{HR} (residues 395-2129), hBrr2^{NC} (residues 395-1324) and hBrr2^{CC} (residues 1282-2136) were produced and purified following previously described protocols (*18*). To monitor interaction of hPrp8^{Jab1} with the various hBrr2 constructs, proteins were mixed with a two-fold molar excess of hPrp8^{Jab1} and analytical gel filtration chromatography was carried out on a Superdex 200 PC 3.2/30 column (GE Healthcare) in 20 mM Tris-HCl, pH 8.0, 200 mM NaCl, 1 mM DTT.

Production and analysis of recombinant yeast proteins

Yeast proteins were used for the majority of functional assays as they are highly homologous to their human counterparts. Furthermore, RP13-linked Prp8 residues are highly conserved across evolution (Fig. 3A) and the severity of retinal degeneration in patients with RP13 mutations correlates with the severity of growth phenotypes associated with corresponding Prp8 mutations in haploid yeast (*10*). yPrp8^{Jab1} (residues 2012-2413) and mutant/truncated versions thereof, were produced in *E. coli* and purified as described previously (*12, 20*). Site-directed mutations were introduced *via* the QuikChange protocol and were verified by sequencing. Full-length yBrr2 containing an N-terminal His_6-tag was produced in yeast INVSc1 cells (Invitrogen) and purified as described (*13*). To monitor interaction of yBrr2 with yPrp8^{Jab1} variants, equimolar amounts (4 µM each) of the proteins were mixed and incubated for 30 min at 4 °C in 50 µl reaction volume, and size exclusion chromatography was subsequently performed with a Superdex 200 PC 3.2/30 column in 40 mM Tris-HCl, pH 7.5, 100 mM NaCl, 2 mM DTT, 5 % glycerol.

Crystallographic analyses

The hBrr2^{HR}-hPrp8^{Jab1} complex was concentrated to 12 mg/ml and crystallized at 4 ºC using the hanging drop vapor diffusion method. Crystals were obtained by mixing 1 µl of protein solution with 0.5 µl of reservoir solution (0.1 M HEPES-NaOH, pH 7.9, 0.2 M $MgCl_2$, 12 % ethanol) and improved by addition of a cocktail of additives (Silver Bullets Bio condition 91;

Hampton Research) dissolved in the gel filtration buffer. Further optimization of crystal quality was achieved by adding to the crystallization drop eight volumes of a solution containing 0.1 M HEPES-NaOH, pH 7.9, 0.2 M $MgCl_2$, 22 % ethanol, 10 % ethylene glycol and exposing the mixtures to air for 30 min.

Crystals were cryo-protected by transfer into a solution containing 0.1 M HEPES-NaOH, pH 7.9, 0.2 M $MgCl_2$, 12 % ethanol, 30 % ethylene glycol and flash-cooled in liquid nitrogen. Diffraction data were collected on a single crystal at beamline 14.2 of the BESSY II storage ring (Berlin, Germany) and processed with XDS (*23*). The structure of the $hBrr2^{HR}$-$hPrp8^{Jab1}$ complex was solved by automated molecular replacement with the program MOLREP from the CCP4 suite (*24*) using the structure coordinates of $hBrr2^{HR}$ (PDB ID 4F91) (*18*) and $yPrp8^{Jab1}$ (PDB ID 2OG4) (*16*) as search models. The structure was refined through several rounds of manual model building in COOT (*25*) and restrained refinement in PHENIX (*26*).

RNA binding studies

His-tag pulldown assays were performed as described previously (*13*), except His-tagged yBrr2 (0.8 µM) and $yPrp8^{Jab1}$ or $yPrp8^{Jab1\text{-}\Delta C16}$ (3 µM) were first combined, followed in some cases by 2 mM ATPγS, and then [^{32}P]-labeled U4/U6 di-snRNA (a mixture of 5 nM labeled and 15 nM non-labeled RNA) was added. Fluorescence anisotropy was performed essentially as described (*18*), except a FAM-5' end-labeled, 24 nt single-stranded RNA (5 nM) was incubated in the presence of 0-400 nM yBrr2 alone or yBrr2 pre-incubated with 1 µM $yPrp8^{Jab1}$ or $yPrp8^{Jab1\text{-}\Delta C16}$ followed by addition of 1 mM ATPγS where indicated. The apparent equilibrium dissociation constants (K_d) for Brr2-RNA complex formation were determined as previously described (*18*).

ATPase and U4/U6 di-snRNA unwinding assays

Steady-state ATPase assays were performed as described (*18*). Briefly, 25 nM yBrr2, 0.5 µM U4/U6 di-snRNA, 0.5 mM ATP and, where indicated, 1 µM of yPrp8^{Jab1} variants were mixed at 20 °C, and the amount of liberated inorganic phosphate was measured using a malachite dye-based kit (PiColorLock™ Gold, Innova Biosciences).

U4/U6 di-snRNA unwinding assays were carried out at 20 °C or 30 °C for 0-50 min essentially as described (*18*), except helicases were incubated alone or with 0.75 µM of yPrp8^{Jab1} or mutants thereof for 15 min at 4 °C prior to addition of RNA. In all experiments, U4 snRNA was radiolabeled. RNA duplex displacement was analyzed by 6 % native PAGE, visualized by autoradiography and quantified as described (*20*). Reannealing of the U4/U6 duplex after strand displacement is not observed under these assay conditions due to the formation of a U6 intra-molecular stem-loop that precludes U4/U6 duplex formation.

To determine the specificity of the yPrp8^{Jab1} effects, 200 nM yBrr2 or 150 nM yPrp22 were pre-incubated with increasing concentrations (0-2 µM) of yPrp8^{Jab1}. U4/U6 duplex (0.5 nM) was subsequently added, followed by 1 mM ATP/$MgCl_2$ to start the reaction, which was then incubated at 20 ºC for 40 min. Time courses of U4/U6 unwinding under multiple turnover conditions at low U4/U6 to Brr2 ratio were assayed with 200 nM yBrr2 in the absence or presence of yPrp8^{Jab1} or mutants thereof and 0.5 nM U4/U6 duplex. The reaction was initiated by the addition of 1 mM ATP/$MgCl_2$ and incubated for the indicated times at 20 °C or 30 °C. Time courses of U4/U6 unwinding under multiple turnover conditions at higher U4/U6 to Brr2 ratio were assayed with 200 nM yBrr2 in the absence or presence of yPrp8^{Jab1} or mutants thereof and 50 nM U4/U6 duplex. The reaction was initiated by the addition of 1 mM ATP/$MgCl_2$ and incubated for the indicated times at 30 °C. The effect of Prp8^{Jab1} on U4/U6 unwinding by the Brr2 N-terminal cassette alone was assayed with 200 nM of an hBrr2 construct comprising only the N-terminal cassette (hBrr2^{NC}) (*18*) in the absence or presence of hPrp8^{Jab1} or hPrp8$^{Jab1\text{-}\Delta C15}$ and 50 nM U4/U6 duplex. The reaction was initiated by the addition of 1 mM ATP/$MgCl_2$ and

incubated for the indicated times at 30 °C. For quantification, data were fit to a single exponential equation: % duplex unwound = A{1-exp(-k_u t)}; A, amplitude of the reaction; k_u, apparent first-order rate constant for unwinding; t, time.

Plasmid shuffling, yeast growth assays and *in vivo* splicing assays

Plasmids encoding wildtype (wt) Prp8 or Prp8 containing the indicated mutations were introduced into a *S. cerevisiae* strain with the wt *PRP8* gene on a counter-selectable plasmid (*27*). Ten-fold serial dilutions of the yeast strains were applied to YPD agar plates and cells were incubated at the indicated temperatures for 2 days. For the analysis of pre-mRNA splicing *in vivo*, total RNA was isolated from the wt and mutant strains grown at 25 °C or 37 °C for 4 h in YPD medium. The levels of spliced and unspliced U3 RNA were analyzed by primer extension analysis using a [^{32}P]-labeled primer complementary to exon 2 (*28*). The ratio of pre-U3 to mature U3 RNA was quantified using a phosphoimager (Molecular Dynamics) and Quantity One software.

Analysis of tri-snRNP levels in yeast cells

Total cell extract was prepared from yeast cells grown at 30°C that express wt Prp8 or the indicated Prp8 temperature sensitive mutant (*29*). Extracts were incubated at 35°C (i.e., the non-permissive temperature for the Prp8 temperature sensitive mutants) for 20 min and then subjected to 10-30% glycerol gradient centrifugation as described (*21*). RNA from every second gradient fraction was isolated and the distribution of the spliceosomal snRNAs was analyzed by Northern blotting with [^{32}P]-labeled probes complementary to yeast U1, U2, U4, U5 or U6 snRNA. Quantification of the levels of U6 and U4 snRNA was performed with a phosphoimager (Molecular Dynamics) and Quantity One software. The distribution of Prp8, Brr2 and Snu114 across the gradient was determined by Western blotting. Immunostaining was performed with antibodies against the corresponding protein and an ECL detection kit (GE Healthcare).

Supplementary Figures

Fig. S1

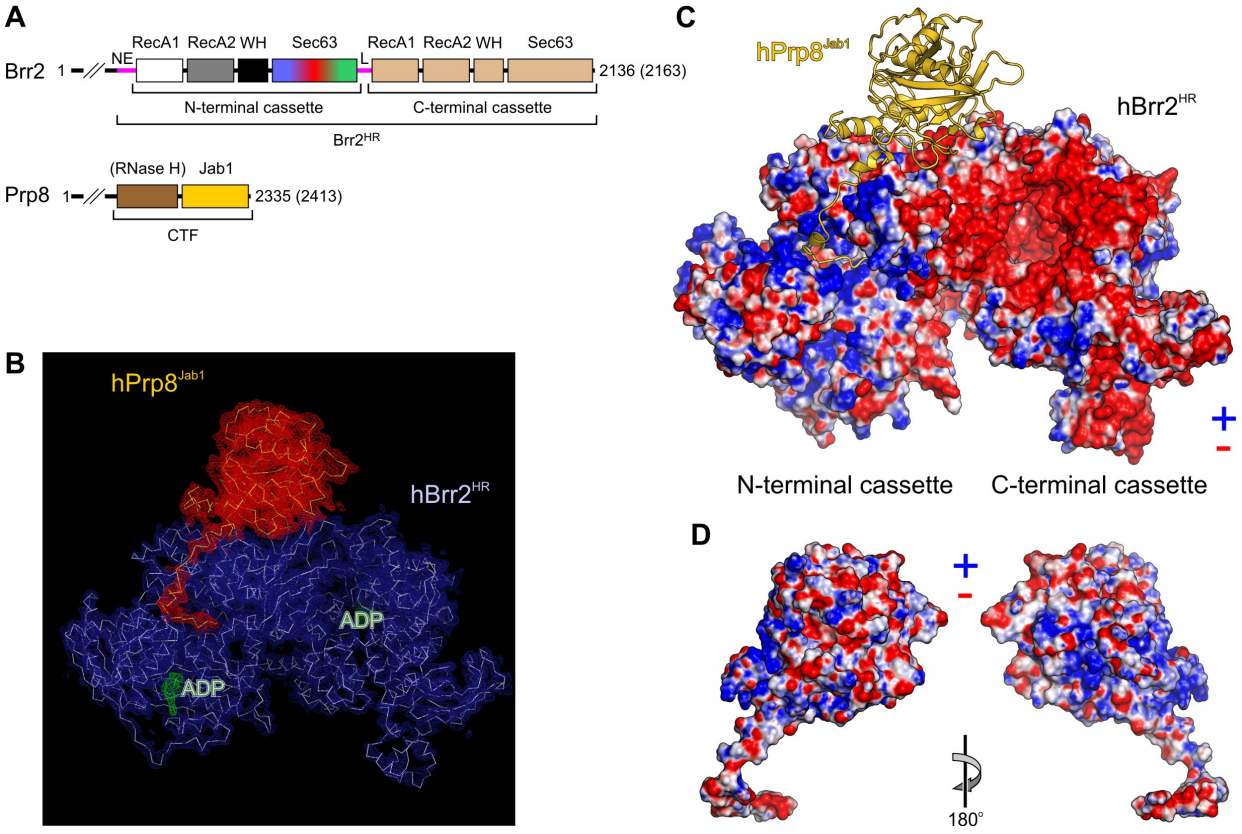

Fig. S1. Electron density and surface electrostatics. (**A**) Domain organization of Brr2 and of a C-terminal fragment (CTF) of Prp8. Domain coloring as in Fig. 1A. NE, N-terminal extension; Sec63 – Sec63 homology units (comprising helical bundle, helix-loop-helix and immunoglobulin-like domains) (*11, 20*); RNase H, RNase H-like domain; Jab1, Jab1/MPN-like domain. The RNase H-like domain is not contained in the present crystal structure. Human (yeast) numbering. (**B**) Simulated annealing composite "omit" electron density contoured at the 1σ level. Molecules are shown as Cα traces (hBrr2^{HR}, light blue; hPrp8^{Jab1}, gold) or sticks (ADP, light green). Indicated ADP represents the ADP portion of ß-nicotinamide adenine dinucleotide added as an additive during crystallization. Density around hBrr2^{HR}, blue; density around hPrp8^{Jab1}, red; density around nucleotides, green. Rotated 30 ° about the horizontal axis (top to

front) compared to Fig. 1A. (**C**) hBrr2^{HR} electrostatic surface (positive, blue; negative, red) with the hPrp8 Jab1 domain shown as a golden ribbon. Rotated 40 ° about the horizontal axis (top to front) compared to Fig. 1A. (**D**) Electrostatic surface of the hPrp8 Jab1 domain in two orthogonal views. The left orientation is the same as in (C). The tail is predominantly negatively-charged, which is suitable for binding the RNA tunnel of Brr2, where under a different situation the negatively-charged sugar-phosphate backbone of the RNA substrate must interact. 5194 Å^2 of combined surface area are buried upon complex formation, 2417 Å^2 between hBrr2^{HR} and the globular part of hPrp8^{Jab1} (residues 2067-2309), 2777 Å^2 between hBrr2^{HR} and the C-terminal tail of hPrp8^{Jab1} (residues 2310-2335). 960 Å^2 of combined surface area are buried between the proximal part of the hPrp8^{Jab1} C-terminal tail (residues 2310-2320) and hBrr2^{HR}, 1817 Å^2 between the distal part of the tail (residue 2321-2335) and hBrr2^{HR}.

Fig. S2

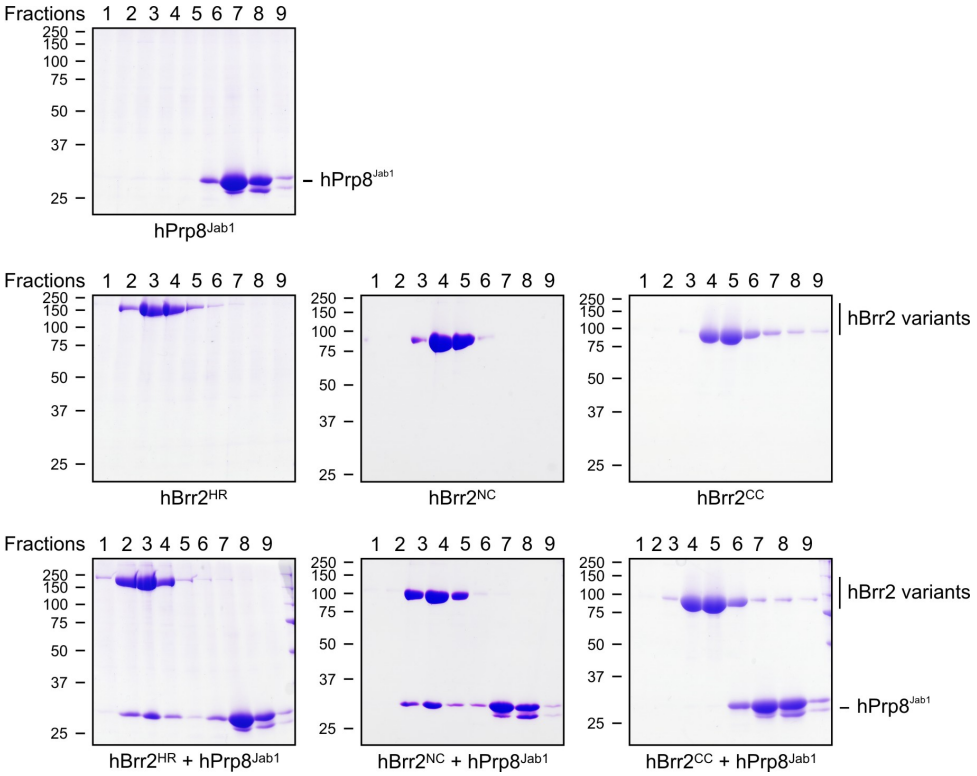

Fig. S2. The human Prp8 Jab1 domain interacts with the N-terminal helicase cassette of hBrr2 in solution. Gel filtration analyses were performed with the indicated individual proteins or protein mixtures. Proteins were mixed at 2:1 ($hPrp8^{Jab1}$:hBrr2 variant) molar ratio prior to size exclusion chromatography, and proteins in the eluted fractions 1-9 (identical in each panel) were analyzed by SDS-PAGE. Numbers on the left indicate molecular mass standards in kD. $hPrp8^{Jab1}$ (residues 2064-2335) co-migrated with a 200 kD fragment of hBrr2 (residues 395-2129) encompassing both helicase cassettes (hBrr2 helicase region; $hBrr2^{HR}$), and with the isolated hBrr2 N-terminal cassette ($hBrr2^{NC}$; residues 395-1324), but not with the isolated C-terminal cassette ($hBrr2^{CC}$; residues 1282-2136). While $yBrr2^{NC}$ was not soluble and could not be tested for interaction with $yPrp8^{Jab1}$, the high conservation of Brr2 sequence and function suggests the same interaction scheme in yeast. Indeed, previous pulldown experiments (*11*) detected only a weak interaction of $yPrp8^{CTF}$ (which contains the Jab1 domain) with $yBrr2^{CC}$.

Fig. S3

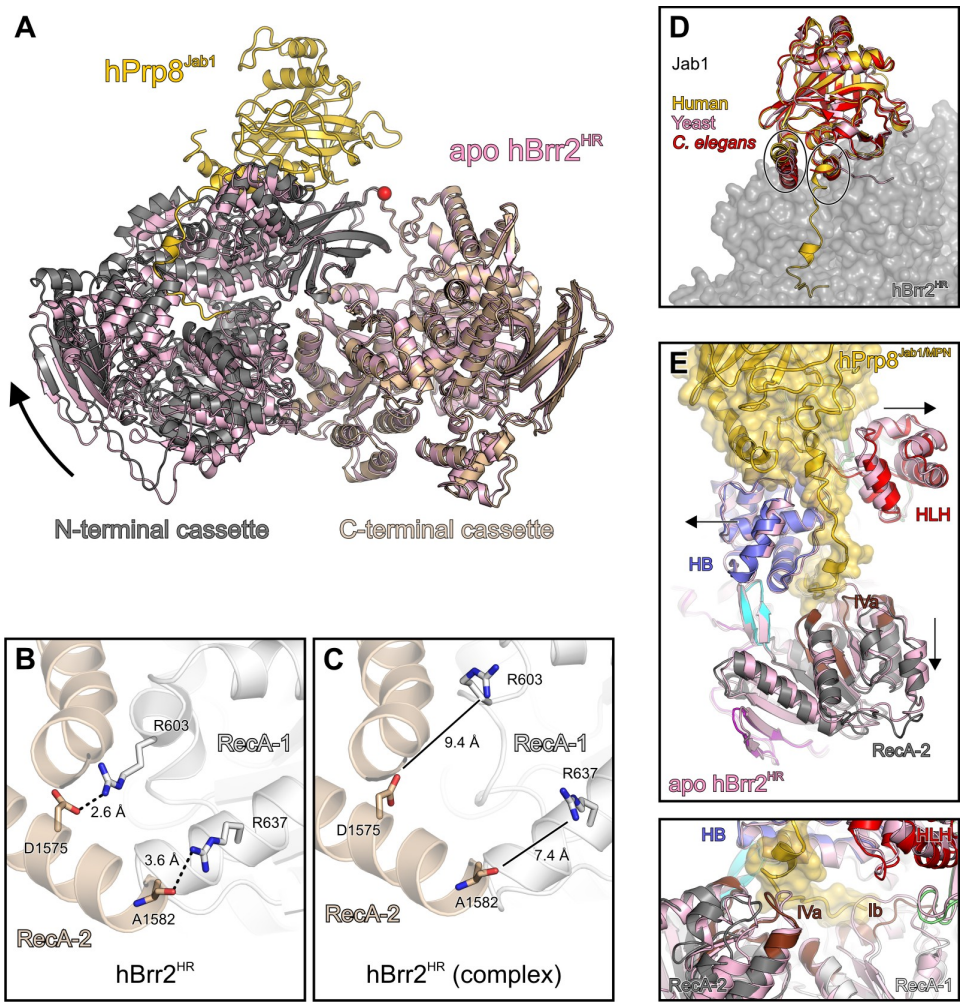

Fig. S3. Conformational changes upon complex formation. (**A**) Superposition of isolated hBrr2^{HR} (pink) and the hBrr2^{HR}-hPrp8^{Jab1} complex (N-terminal cassette – grey; C-terminal cassette – beige; hPrp8^{Jab1} – gold) according to the C-terminal cassettes of the hBrr2^{HR} molecules. The arrow indicates an apparent movement of the N-terminal cassette about a pivot point in the linker (red sphere) relative to the C-terminal cassette upon hPrp8^{Jab1} binding. Orientation as in Fig. 1A. (**B**) Close-up of contacts between the N-terminal RecA-1 domain (light grey) and the C-terminal RecA-2 domain (beige), which upon mutation led to severely reduced helicase activity in hBrr2^{HR} (*18*). Dashed lines indicate hydrogen bonds or salt bridges. Contacting residues are

labeled and contact distances are indicated. Rotated 180 ° about the vertical axis compared to (A). (**C**) The same region of hBrr2^{HR} in the hPrp8^{Jab1} complex. Corresponding distances as in (B) are indicated. Rotated 180 ° about the vertical axis compared to (A). The structural changes shown in (A-C) upon complex formation indicate that the interaction between N- and C-terminal cassettes in Brr2 is partially flexible, which may have important implications for the mechanism of U4/U6 unwinding by Brr2. Mutations in the linker, the intercassette RecA-contacts and the ATP pocket of the C-terminal cassette have severe effects on hBrr2^{HR} ATPase and helicase activity (*18*). During cycles of RNA duplex unwinding, the intercassette RecA-contacts may have to be intermittently broken and re-formed, e.g. to allow repositioning of the RNA bound at the N-terminal cassette. Close association of the linker with either cassette would allow it to tightly fasten the cassettes at one side, which in turn would enable a portion of the linker between the cassette contact regions to act like a hinge during opening and closing motions on the RecA-side. A bound nucleotide would stabilize the C-terminal cassette, allowing it to act as a scaffold relative to which the N-terminal cassette can move. (**D**) The structures of isolated Prp8 Jab1 domains from yeast (pink; PDB ID 2OG4) (*16*) and *C. elegans* (red; PDB ID 2P87) (*17*) superimposed on the human Prp8 Jab1 domain (gold) in complex with hBrr2^{HR} (grey semi-transparent surface). The structure of isolated hPrp8^{Jab1} is not available but most likely closely resembles those of yeast and *C. elegans* Prp8^{Jab1} due to the high sequence similarity of these proteins. The structure of hPrp8^{Jab1} in complex with hBrr2^{HR} is similar to the structure of isolated yPrp8^{Jab1} (rmsd of 1.48 Å for 226 Cα atoms) and *C. elegans* Prp8^{Jab1} (rmsd of 1.00 Å for 238 Cα atoms), with significant deviations only in elements that directly contact hBrr2^{HR} (circled). Additionally, the C-terminal tail of the Jab1 domain was flexible and only partially resolved in the structures of the domain in isolation. Rotated 40 ° clockwise about the vertical axis and 20 ° about the horizontal axis (top to front) compared to Fig. 1A. (**E**) Structural changes in hBrr2^{HR} upon binding of hPrp8^{Jab1}. Top panel – domain movements. The hBrr2^{HR}-hPrp8^{Jab1} complex is colored as before, isolated hBrr2^{HR} is shown in pink. Rotated 70 ° clockwise about the vertical

axis and 50 ° about the horizontal axis (top to front) compared to Fig. 1A. Bottom panel – local conformational adjustments. Rotated 30 ° about the horizontal axis (top to front) compared to Fig. 1A. Individual domains of hBrr2^{HR} retain similar structures in the complex as in the isolated protein (rmsd's ranging from 0.51 Å for the N-terminal IG domains to 1.13 Å for the N-terminal RecA-2 domains). However, changes in the positioning of certain domains and local conformational adjustments in a number of elements upon hPrp8^{Jab1} binding are observed. Essentially no structural rearrangements are seen in those regions of the N-terminal HB and IG domains of hBrr2^{HR} that are contacted by the globular part of hPrp8^{Jab1}. In contrast, the entire HLH domain, the front end of the HB domain and the upper tip of the RecA-2 domain are pushed away from each other in order to accommodate the C-terminal tail of hPrp8^{Jab1} (arrows in E). In addition, the conformations of RNA-binding motifs IVa and Ib adapt to the central and terminal portions of the C-terminal tail, respectively (lower panel in E). Taken together, hBrr2^{HR} and hPrp8^{Jab1} bind to each other by a mixed lock-and-key and induced fit interaction mode.

Fig. S4

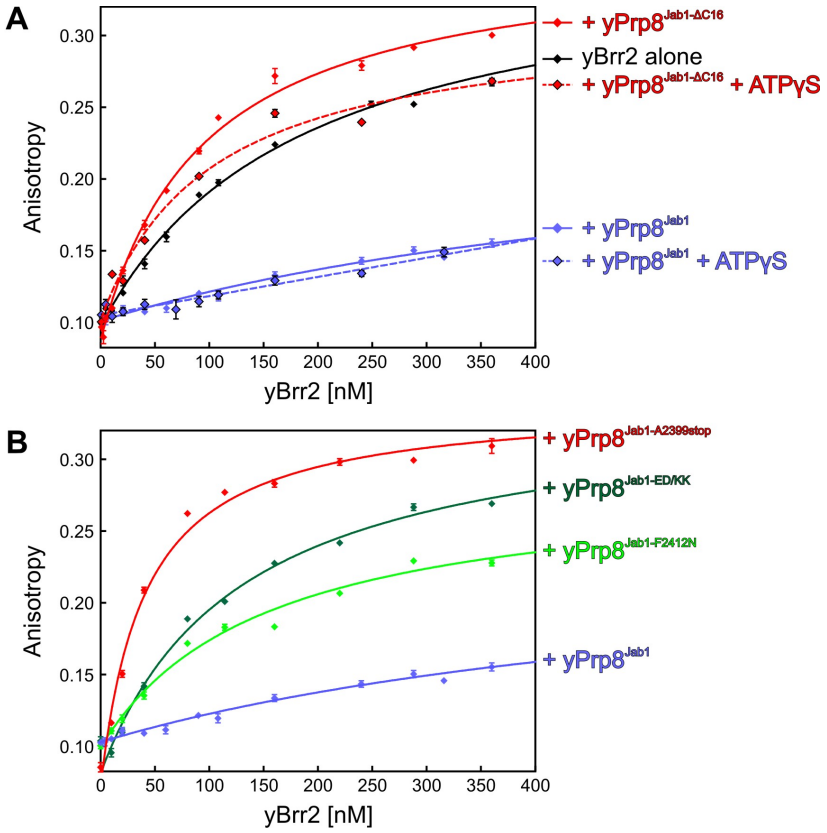

Fig. S4. Effects on Brr2 RNA binding. (**A**) Effect of yPrp8^{Jab1} on the binding of yBrr2 to a 24 nt RNA monitored by fluorescence anisotropy. For technical reasons (due to the high molecular weight of U4/U6 di-snRNA), these experiments could not be conducted with U4/U6 di-snRNA. Error bars represent SEMs of three independent experiments. yBrr2-RNA dissociation constants (K_d): K_d(yBrr2) = 183.7 ± 13.3 nM; K_d(yBrr2-yPrp8^{Jab1}) > 600 nM (+/-ATPγS); K_d(yBrr2-yPrp8$^{Jab1\text{-}\Delta C16}$) = 95 ± 6 nM (- ATPγS) or 100.8 ± 13.2 nM (+ ATPγS). (**B**) Effect of yPrp8^{Jab1} mutations on the binding of yBrr2 to a 24 nt RNA monitored by fluorescence anisotropy. Error bars represent SEMs of three independent experiments. yPrp8$^{Jab1\text{-}ED/KK}$, yPrp8$^{Jab1\text{-}E2407K/D2410K}$ variant. yBrr2-RNA and [yBrr2-yPrp8^{Jab1}]-RNA dissociation constants (K_d): K_d(yBrr2-yPrp8^{Jab1}) as in (A); K_d(yBrr2-yPrp8$^{Jab1\text{-}A2399stop}$) = 40.6 ± 2.9 nM; K_d(yBrr2-yPrp8$^{Jab1\text{-}F2412N}$) = 131.8 ± 13.2 nM; K_d(yBrr2-yPrp8$^{Jab1\text{-}ED/KK}$) = 137.3 ± 11.0 nM.

Fig. S5

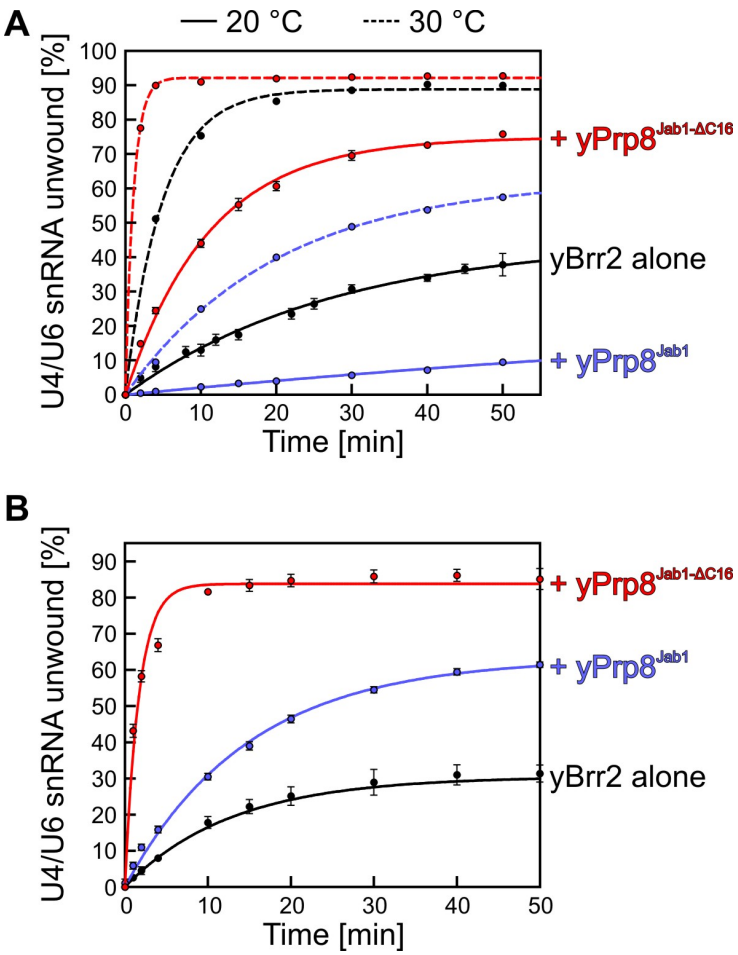

Fig. S5. Effects of yPrp8^{Jab1} or yPrp8$^{Jab1\text{-}\Delta C16}$ on yBrr2-mediated U4/U6 unwinding. (**A**) U4/U6 unwinding at low U4/U6 (0.5 nM) to yBrr2 (200 nM) ratio (quantified data from Fig. 2C). Data were fit to a single exponential equation: % duplex unwound = A{1-exp(-k_u t)}; A, amplitude of the reaction; k_u, apparent first-order rate constant for unwinding; t, time. Solid lines, 20 °C; dashed lines, 30 °C. yBrr2 alone, black; yBrr2-yPrp8^{Jab1}, blue; yBrr2-yPrp8$^{Jab1\text{-}\Delta C16}$, red. Kinetic parameters at 20 °C: k_u(yBrr2) = 0.034 ± 0.004 min^{-1}; A(yBrr2) = 45.3 ± 2.9; k_u(yBrr2-yPrp8^{Jab1}) = 0.01 ± 0.01 min^{-1}; A(yBrr2-yPrp8^{Jab1}) = 31.6 ± 9.2; k_u(yBrr2-yPrp8$^{Jab1\text{-}\Delta C16}$) = 0.09 ± 0.01 min^{-1}; A(yBrr2-yPrp8$^{Jab1\text{-}\Delta C16}$) = 75.0 ± 0.9. (**B**) U4/U6 unwinding at higher U4/U6 (50 nM) to yBrr2 (200 nM) ratio at 30 °C (quantified data from Fig. 2D). Data were fit to a single exponential equation:

% duplex unwound = A{1-exp(-k_u t)}; A, amplitude of the reaction; k_u, apparent first-order rate constant for unwinding; t, time. yBrr2 alone, black; yBrr2-yPrp8^{Jab1}, blue; yBrr2-yPrp8$^{Jab1\text{-}\Delta C16}$, red). Kinetic parameters: k_u(yBrr2) = 0.07 ± 0.01 min^{-1}, A(yBrr2) = 32.1 ± 1.3; k_u(yBrr2/yPrp8^{Jab1}) = 0.06 ± 0.01 min^{-1}, A(yBrr2/yPrp8^{Jab1}) = 63.3 ± 0.9; k_u(yBrr2/yPrp8$^{Jab1\text{-}\Delta C16}$) = 0.59 ± 0.04 min^{-1}, A(yBrr2/yPrp8$^{Jab1\text{-}\Delta C16}$) = 83.7 ± 1.3.

Fig. S6

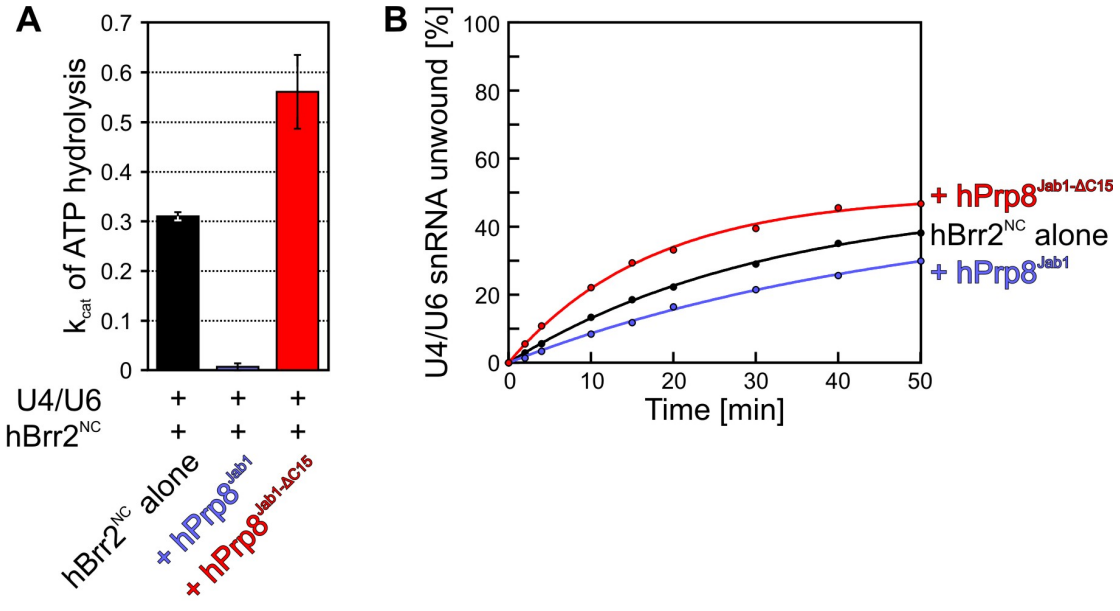

Fig. S6. The C-terminal helicase cassette of Brr2 is required for its regulation by $Prp8^{Jab1}$. (**A**) RNA-stimulated steady state ATPase activity of the hBrr2 N-terminal cassette ($hBrr2^{NC}$) alone (black bar) or in the presence of $hPrp8^{Jab1}$ (blue bar) or $hPrp8^{Jab1\text{-}\Delta C15}$ (red bar). Error bars represent SEMs for two independent experiments. Due to solubility problems with the N-terminal cassette of yBrr2, human proteins were used in these studies. The ATPase activity of isolated $hBrr2^{NC}$ was still inhibited by $hPrp8^{Jab1}$ and stimulated ca. 2-fold by $hPrp8^{Jab1}$ lacking the last 15 residues ($hPrp8^{Jab1\text{-}\Delta C15}$), consistent with reduced binding of RNA to $hBrr2^{NC}$ in the presence of the C-terminal tail of $hPrp8^{Jab1}$. (**B**) Time courses of U4/U6 duplex (50 nM) unwinding by $hBrr2^{NC}$ in the absence (black line) or presence of $hPrp8^{Jab1}$ (blue line) or $hPrp8^{Jab1\text{-}\Delta C15}$ (red line) at 30 °C. Data were fit to a single exponential equation: % duplex unwound = A{1-exp(-k_u t)}; A, amplitude of the reaction; k_u, apparent first-order rate constant for unwinding; t, time. Kinetic parameters: $k_u(hBrr2^{NC})$ = 0.03 ± 0.01; $A(hBrr2^{NC})$ = 48.1 ± 1.0; $k_u(hBrr2^{NC}\text{-}hPrp8^{Jab1})$ = 0.02 ± 0.01; $A(hBrr2^{NC}\text{-}hPrp8^{Jab1})$ = 46.7 ± 2.8; $k_u(hBrr2^{NC}\text{-}hPrp8^{Jab1\text{-}\Delta C15})$ = 0.06 ± 0.01; $A(hBrr2^{NC}\text{-}hPrp8^{Jab1\text{-}\Delta C15})$ = 49.3 ± 1.0. Thus, $hPrp8^{Jab1}$ and $hPrp8^{Jab1\text{-}\Delta C15}$ had only

minimal effects on U4/U6 unwinding by hBrr2^{NC} under these conditions, as well as at lower RNA concentrations (data not shown). This loss of regulatory potential suggests that cooperative movement of both cassettes might be required for insertion of the Jab1 tail into the RNA-binding tunnel of Brr2 and/or that modulation of Brr2 by Prp8^{Jab1} could involve structural changes in the N-terminal cassette that are at least in part facilitated *via* the C-terminal cassette.

Fig. S7

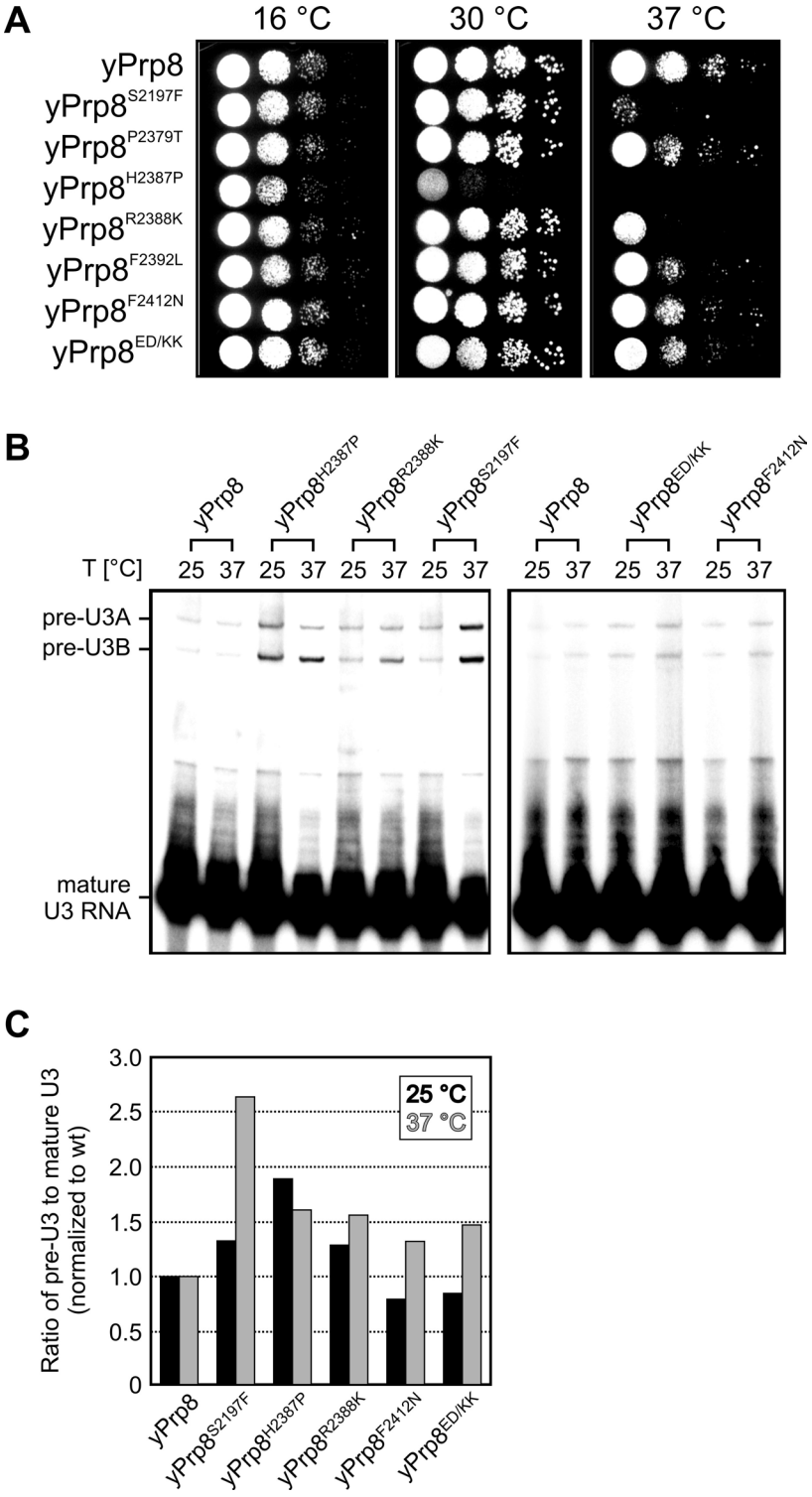
A
16 °C
30 °C
37 °C
yPrp8
yPrp8S2197F
yPrp8P2379T
yPrp8H2387P
yPrp8R2388K
yPrp8F2392L
yPrp8F2412N
yPrp8ED/KK
B
yPrp8
yPrp8H2387P
yPrp8R2388K
yPrp8S2197F
yPrp8
yPrp8ED/KK
yPrp8F2412N
T [°C]
25 37 25 37 25 37 25 37 25 37 25 37 25 37
pre-U3A
pre-U3B
mature
U3 RNA
C
Ratio of pre-U3 to mature U3
(normalized to wt)
3.0
2.5
2.0
1.5
1.0
0.5
0
25 °C
37 °C
yPrp8
yPrp8S2197F
yPrp8H2387P
yPrp8R2388K
yPrp8F2412N
yPrp8ED/KK

Fig. S7. Effects of RP-linked mutations in Prp8^{Jab1} on yeast cell growth and splicing *in vivo*. Plasmids encoding wt yPrp8 or yPrp8 containing the indicated mutations were shuffled into a strain with the wt *yPRP8* gene on a counter-selectable plasmid. (**A**) Serial dilutions of the indicated yeast strains were applied to YPD agar plates and cells were incubated at the indicated temperatures for 1-2 days. (**B**) Total RNA was harvested from the wt and or mutant yeast strain grown at the indicated temperature for 4 h in YPD medium. The levels of spliced and unspliced U3 RNA were analyzed by primer extension analysis using a [^{32}P]-labeled primer complementary to exon 2. Primer extension products were separated by denaturing PAGE and visualized by autoradiography. This assay allows detection of a block in splicing solely prior to or during the first splicing transesterification reaction. (**C**) Quantification of the ratio of pre-U3 to mature U3 (normalized to the wt) at 25 °C (black bars) and 37 °C (grey bars).

Fig. S8

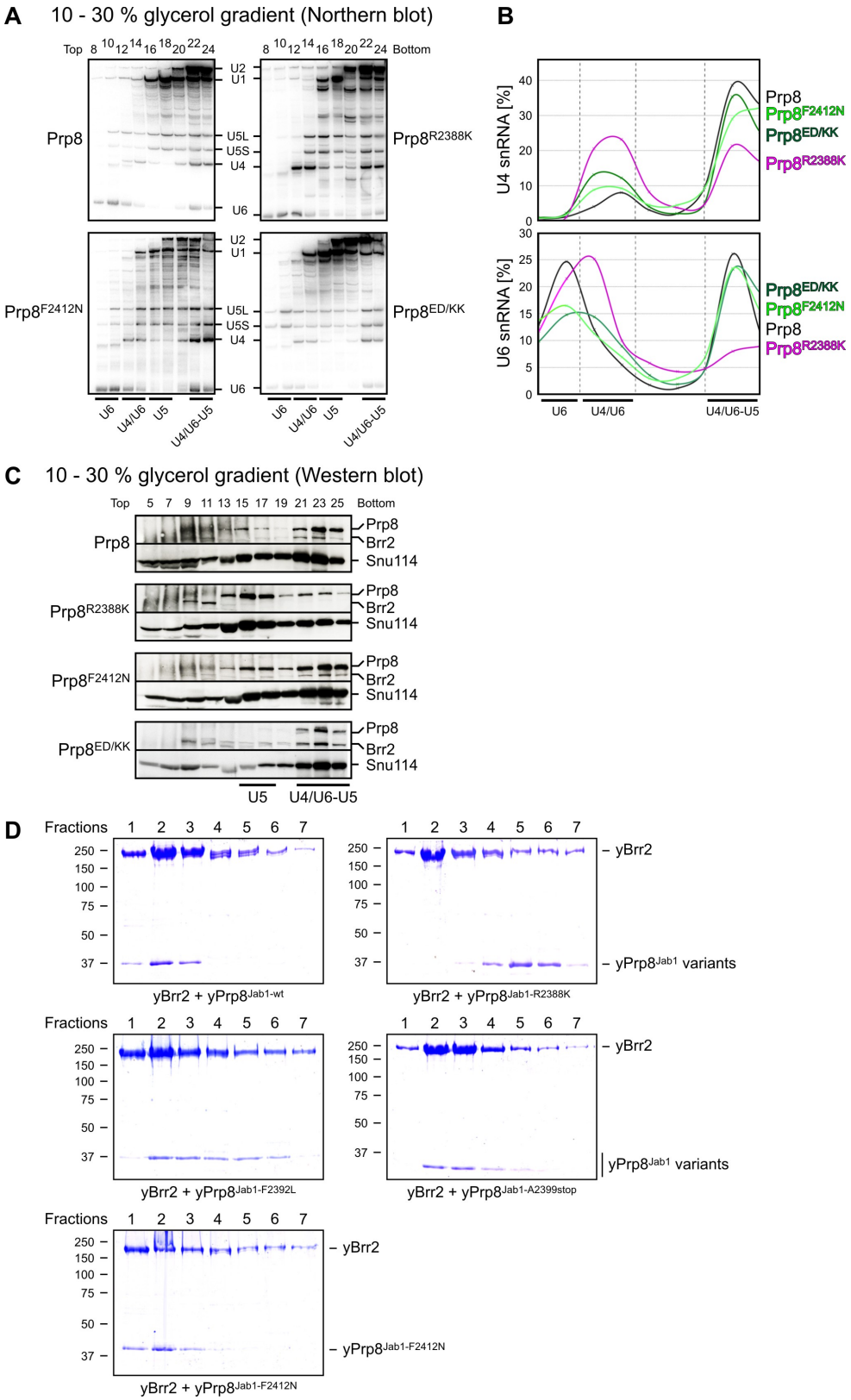
A
10 - 30 % glycerol gradient (Northern blot)
Top
Bottom
Prp8
Prp8R2388K
Prp8F2412N
Prp8ED/KK
U2
U1
U5L
U5S
U4
U6
U6
U4/U6
U5
U4/U6-U5
B
U4 snRNA [%]
U6 snRNA [%]
Prp8
Prp8F2412N
Prp8ED/KK
Prp8R2388K
U6
U4/U6
U4/U6-U5
C
10 - 30 % glycerol gradient (Western blot)
Top
Bottom
Prp8
Brr2
Snu114
U5
U4/U6-U5
D
Fractions
yBrr2
yPrp8Jab1 variants
yBrr2 + yPrp8Jab1-wt
yBrr2 + yPrp8Jab1-R2388K
yBrr2 + yPrp8Jab1-F2392L
yBrr2 + yPrp8Jab1-A2399stop
yPrp8Jab1-F2412N
yBrr2 + yPrp8Jab1-F2412N

Fig. S8. Effects of RP-linked mutations in Prp8 on yeast U4/U6-U5 tri-snRNP levels and on the association of the Prp8 Jab1 domain with Brr2. (**A**) Distribution of yeast spliceosomal snRNPs on glycerol gradients. Total cell extracts were prepared from yeast cells grown at 30 °C expressing wt yPrp8 or Prp8 with the R2388K, F2412N or E2407K/D2410K (ED/KK) mutations. Extracts were incubated at 35 °C for 20 min and then subjected to 10-30 % glycerol gradient centrifugation. Gradients were fractionated, RNA was isolated from the even-numbered fractions and analyzed by Northern blotting. The positions of U1, U2, U4, U5 and U6 snRNAs are indicated. The positions of U6 snRNP, U4/U6 di-snRNP and U4/U6-U5 tri-snRNP are indicated at the bottom. (**B**) Profiles of the U4 and U6 snRNA distributions across the gradients. (**C**) Western blot of proteins isolated from the odd-numbered gradient fractions (indicated at the top) containing extract from cells expressing wt yPrp8 or the R2388K or F2412N mutants thereof. Blots were immunostained with antibodies against yPrp8 and yBrr2 (top panel) or against ySnu114 (lower panel). Consistent with previous studies (*21*), the amount of tri-snRNP relative to U4/U6 di-snRNP was reduced in cells expressing the $Prp8^{R2388K}$ variant, and Brr2 association with U5 or the tri-snRNP was similarly diminished. In contrast, the amount of tri-snRNP relative to U4/U6 was not altered in cells expressing $Prp8^{F2412N}$ or $Prp8^{E2407K/D2410K}$, and Brr2 association was not affected. Thus, the *in vivo* effects of these mutations, which based on our structure are expected to destabilize the interaction of Prp8's tail with Brr2, can be attributed to misregulation of Brr2 during splicing, rather than a defect in U5 or tri-snRNP formation. (**D**) Interaction of various $yPrp8^{Jab1}$ mutants with yBrr2 monitored by gel filtration. Seven identical fractions were analyzed. Numbers on the left, molecular mass standards in kD.

Fig. S9

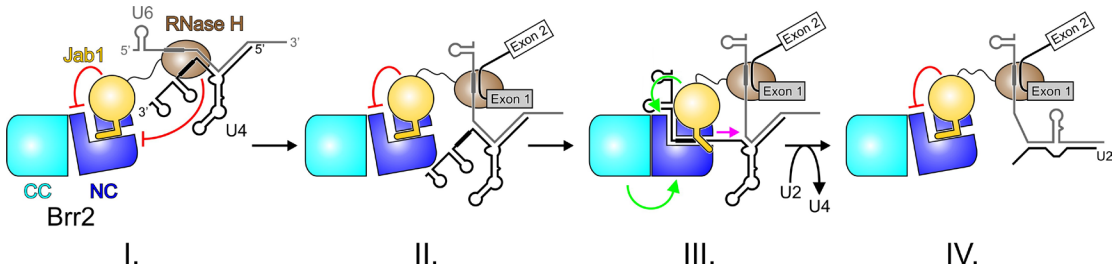

Fig. S9. Working model for the regulation of Brr2 by the Prp8 RNase H and Jab1 domains during pre-mRNA splicing. Red lines, inhibitory effects; green arrows, stimulatory effects. (**I.**) Inhibited state in the U4/U6-U5 tri-snRNP and during early spliceosome assembly achieved by competitive binding of a single-stranded U4 snRNA region upstream of stem I (thick black line) *via* the RNase H domain (*13*) and by blocking the RNA-binding tunnel and disruption of the N-terminal cassette (NC) - C-terminal cassette (CC) interactions (see fig. S3A-C) *via* the Prp8 Jab1 domain. (**II.**) State after release of U4 snRNA from RNase H with Brr2 still blocked *via* the Prp8 Jab1 domain. The conserved U6 ACAGAG box (thick grey line) has taken over base pairing of the 5' splice site from U1 snRNA. It is likely but not certain that the block by the Prp8 RNase H domain is released before the block by the Prp8 Jab1 domain. (**III.**) Brr2 stimulation during spliceosome catalytic activation *via* the globular part and proximal tail of Prp8 Jab1 domain and by direct interaction of N- and C-terminal cassettes (*18*). Magenta arrow, movement of Brr2 on U4 snRNA. (**IV.**) The Prp8 Jab1 domain may again block Brr2 after spliceosome catalytic activation. Presently, there is no direct evidence that the blocks implemented *via* the Prp8 RNase H and Jab1 domains are released in a stepwise fashion or that the Prp8 C-terminal tail returns to the Brr2 RNA-binding tunnel after spliceosome activation.

Fig. S10

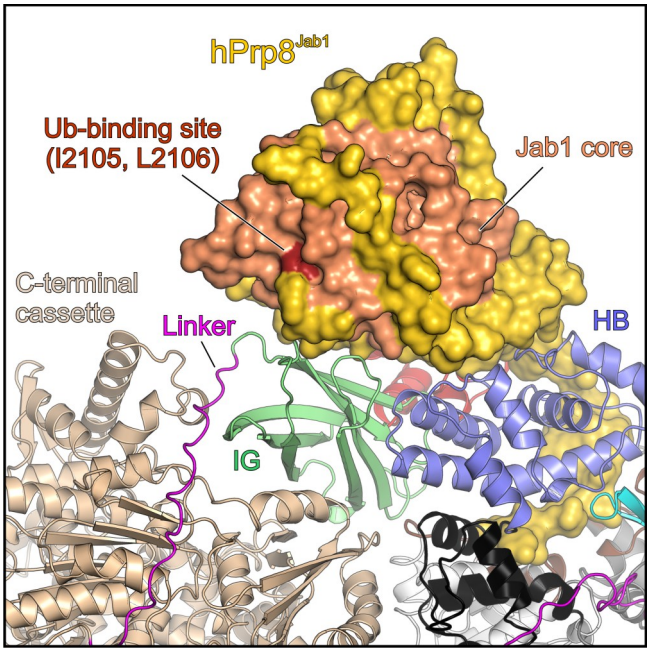

Fig. S10. Potential role of Prp8^{Jab1} de-ubiquitination in triggering de-repression of Brr2 activity. Core of the hPrp8 Jab1 domain, peach; residues I2105 and L2106 of hPrp8^{Jab1}, brick red. Other coloring as before. Rotated 180 ° about the vertical axis compared to Fig. 1A. The release of the C-terminal tail from Brr2's RNA-binding tunnel could be achieved by altering the posttranslational modification status of Prp8. Previous studies have suggested that ubiquitination of Prp8 negatively regulates U4/U6 unwinding by Brr2 (*30*). In yPrp8^{Jab1}, residues V2184 and L2185 have been implicated in ubiquitin binding (*31*), and the corresponding residues of hPrp8 (I2105 and L2106) are located on the backside of the Jab1 domain that is unobstructed in the hBrr2^{HR}-hPrp8^{Jab1} complex. Ubiquitin bound at this site could concomitantly interact with the neighboring N-terminal IG domain or the intercassette linker, thereby eliciting conformational changes that could enhance the negative regulation of Brr2 by Prp8^{Jab1} either by stabilizing the Prp8 C-terminal tail in the RNA-binding tunnel of Brr2 and/or by disrupting intercassette contacts important for Brr2 helicase activity. Thus, deubiquitination of Prp8 constitutes a possible signal *in vivo* that may trigger release of the Prp8 C-terminal peptide from

Brr2 and thereby allow Brr2 to bind its RNA substrate. Alternatively, other spliceosomal proteins, such as Snu114 (*6*), may elicit conformational changes in Brr2 that lead to release of the Prp8 C-terminal tail. As Snu114 has been shown to directly bind $Prp8^{Jab1}$ (*16-17*) this interaction could also free Brr2 for spliceosome activation. Because there is one copy each of Brr2, Prp8 (and thus its Jab1 domain) and U4/U6 in a spliceosome, we suggest that such triggers, rather than general binding equilibria, provide directionality to Brr2 regulation during splicing *in vivo*.

Supplementary Tables

Table S1. Crystallographic statistics

Data collection	
Wavelength (Å)	0.91841
Space group	$P4_22_12$
Unit cell (Å)	
a,b	240.0
c	201.1
Resolution (Å)*	50.0-3.6 (3.80-3.60)
Reflections	
Unique	68276 (10791)
Completeness (%)	99.8 (99.2)
Redundancy	7.5 (7.6)
$\mathbf{R_{sym}\ (I)}$†	17.0 (72.5)
I/σ	14.4 (2.4)
Refinement	
Resolution (Å)	50.0-3.6 (3.65-3.60)
Reflections	
Number	68248 (2605)
Completeness (%)	99.8 (97.0)
Test set (%)	5
R-factors‡	
R_{work}	19.8 (31.6)
R_{free}	23.2 (35.6)
Ramachandran plot	
Favored	94.77
Allowed	5.03
Outlier	0.02
Rmsd§ **geometry**	
Bonds (Å)	0.007
Angles (°)	1.158
PDB ID	4KIT

* Values for the highest resolution shell in parentheses.

† $R_{sym}(I) = (\Sigma_{hkl}\Sigma_i[|I_i(hkl) - \langle I(hkl)\rangle|] / \Sigma_{hkl}\Sigma_i I_i(hkl)$, in which $I_i(hkl)$ – intensity of the i^{th} measurement of reflection hkl; $\langle I(hkl)\rangle$ – average value of the intensity of reflection hkl for all i measurements.

‡ $R_{work} = \Sigma_{hkl}[||F_{obs}| - k|F_{calc}||] / \Sigma_{hkl}|F_{obs}|$; $R_{free} = \Sigma_{hkl\in T}[||F_{obs}| - k|F_{calc}||] / \Sigma_{hkl\in T}|F_{obs}|$; $hkl\in T$ – test set; F_{obs}, F_{calc} – observed and calculated (from model) structure factor amplitudes.

§ Rmsd - root-mean-square deviation.

Table S2. Kinetics of U4/U6 unwinding

Proteins	**A**	k_u [min^{-1}]
yBrr2	32.2 ± 1.3	0.08 ± 0.01
yBrr2-yPrp8^{Jab1}	63.1 ± 0.7	0.06 ± 0.01
yBrr2-yPrp8$^{Jab1\text{-}A2399stop}$	86.3 ± 0.7	0.50 ± 0.02
yBrr2/yPrp8$^{Jab1\text{-}F2412N}$	85.4 ± 1.4	0.33 ± 0.03
yBrr2-yPrp8$^{Jab1\text{-}ED/KK}$	94.9 ± 0.1	1.50 ± 0.02

Data from Brr2-mediated U4/U6 unwinding assays in the absence and presence of Prp8^{Jab1} variants (Fig. 3H) were fit to a single exponential equation: % duplex unwound = A{1-exp(-k_u t)}; A, amplitude of the reaction; k_u, apparent first-order rate constant for unwinding; t, time. Errors represent SEMs of at least two independent experiments.

References and Notes

1. M. C. Wahl, C. L. Will, R. Lührmann, The spliceosome: Design principles of a dynamic RNP machine. *Cell* **136**, 701 (2009). doi:10.1016/j.cell.2009.02.009 Medline

2. B. Laggerbauer, T. Achsel, R. Lührmann, The human U5-200kD DEXH-box protein unwinds U4/U6 RNA duplices in vitro. *Proc. Natl. Acad. Sci. U.S.A.* **95**, 4188 (1998). doi:10.1073/pnas.95.8.4188 Medline

3. P. L. Raghunathan, C. Guthrie, RNA unwinding in U4/U6 snRNPs requires ATP hydrolysis and the DEIH-box splicing factor Brr2. *Curr. Biol.* **8**, 847 (1998). doi:10.1016/S0960-9822(07)00345-4 Medline

4. D. H. Kim, J. J. Rossi, The first ATPase domain of the yeast 246-kDa protein is required for in vivo unwinding of the U4/U6 duplex. *RNA* **5**, 959 (1999). doi:10.1017/S135583829999012X Medline

5. D. Hahn, G. Kudla, D. Tollervey, J. D. Beggs, Brr2p-mediated conformational rearrangements in the spliceosome during activation and substrate repositioning. *Genes Dev.* **26**, 2408 (2012). doi:10.1101/gad.199307.112 Medline

6. E. C. Small, S. R. Leggett, A. A. Winans, J. P. Staley, The EF-G-like GTPase Snu114p regulates spliceosome dynamics mediated by Brr2p, a DExD/H box ATPase. *Mol. Cell* **23**, 389 (2006). doi:10.1016/j.molcel.2006.05.043 Medline

7. J. B. Fourmann *et al*., Dissection of the factor requirements for spliceosome disassembly and the elucidation of its dissociation products using a purified splicing system. *Genes Dev.* **27**, 413 (2013). doi:10.1101/gad.207779.112 Medline

8. A. N. Kuhn, E. M. Reichl, D. A. Brow, Distinct domains of splicing factor Prp8 mediate different aspects of spliceosome activation. *Proc. Natl. Acad. Sci. U.S.A.* **99**, 9145 (2002). doi:10.1073/pnas.102304299 Medline

9. A. N. Kuhn, D. A. Brow, Suppressors of a cold-sensitive mutation in yeast U4 RNA define five domains in the splicing factor Prp8 that influence spliceosome activation. *Genetics* **155**, 1667 (2000). Medline

10. C. Maeder, A. K. Kutach, C. Guthrie, ATP-dependent unwinding of U4/U6 snRNAs by the Brr2 helicase requires the C terminus of Prp8. *Nat. Struct. Mol. Biol.* **16**, 42 (2009). doi:10.1038/nsmb.1535 Medline

11. L. Zhang *et al*., Structural evidence for consecutive Hel308-like modules in the spliceosomal ATPase Brr2. *Nat. Struct. Mol. Biol.* **16**, 731 (2009). doi:10.1038/nsmb.1625 Medline

12. G. Weber *et al*., Mechanism for Aar2p function as a U5 snRNP assembly factor. *Genes Dev.* **25**, 1601 (2011). doi:10.1101/gad.635911 Medline

13. S. Mozaffari-Jovin *et al*., The Prp8 RNase H-like domain inhibits Brr2-mediated U4/U6 snRNA unwinding by blocking Brr2 loading onto the U4 snRNA. *Genes Dev.* **26**, 2422 (2012). doi:10.1101/gad.200949.112 Medline

14. D. Mordes *et al*., Pre-mRNA splicing and retinitis pigmentosa. *Mol. Vis.* **12**, 1259 (2006). Medline

15. K. V. Towns *et al*., Prognosis for splicing factor PRPF8 retinitis pigmentosa, novel mutations and correlation between human and yeast phenotypes. *Hum. Mutat.* **31**, E1361 (2010). doi:10.1002/humu.21236 Medline

16. V. Pena, S. Liu, J. M. Bujnicki, R. Lührmann, M. C. Wahl, Structure of a multipartite protein-protein interaction domain in splicing factor prp8 and its link to retinitis pigmentosa. *Mol. Cell* **25**, 615 (2007). doi:10.1016/j.molcel.2007.01.023 Medline

17. L. Zhang *et al*., Crystal structure of the C-terminal domain of splicing factor Prp8 carrying retinitis pigmentosa mutants. *Protein Sci.* **16**, 1024 (2007). doi:10.1110/ps.072872007 Medline

18. K. F. Santos *et al*., Structural basis for functional cooperation between tandem helicase cassettes in Brr2-mediated remodeling of the spliceosome. *Proc. Natl. Acad. Sci. U.S.A.* **109**, 17418 (2012). doi:10.1073/pnas.1208098109 Medline

19. Materials and methods are available as supplementary materials on *Science* Online.

20. V. Pena *et al*., Common design principles in the spliceosomal RNA helicase Brr2 and in the Hel308 DNA helicase. *Mol. Cell* **35**, 454 (2009). doi:10.1016/j.molcel.2009.08.006 Medline

21. K. L. Boon *et al*., prp8 mutations that cause human retinitis pigmentosa lead to a U5 snRNP maturation defect in yeast. *Nat. Struct. Mol. Biol.* **14**, 1077 (2007). doi:10.1038/nsmb1303 Medline

22. D. J. Fitzgerald *et al*., Protein complex expression by using multigene baculoviral vectors. *Nat. Methods* **3**, 1021 (2006). doi:10.1038/nmeth983 Medline

23. W. Kabsch, Automatic processing of rotation diffraction data from crystals of initially unknown symmetry and cell constants. *J. Appl. Cryst.* **26**, 795 (1993). doi:10.1107/S0021889893005588

24. A. Vagin, A. Teplyakov, Molecular replacement with MOLREP. *Acta Crystallogr. D Biol. Crystallogr.* **66**, 22 (2010). doi:10.1107/S0907444909042589 Medline

25. P. Emsley, K. Cowtan, Coot: model-building tools for molecular graphics. *Acta Crystallogr. D Biol. Crystallogr.* **60**, 2126 (2004). doi:10.1107/S0907444904019158 Medline

26. P. D. Adams *et al*., PHENIX: Building new software for automated crystallographic structure determination. *Acta Crystallogr. D Biol. Crystallogr.* **58**, 1948 (2002). doi:10.1107/S0907444902016657 Medline

27. V. Pena, A. Rozov, P. Fabrizio, R. Lührmann, M. C. Wahl, Structure and function of an RNase H domain at the heart of the spliceosome. *EMBO J.* **27**, 2929 (2008). doi:10.1038/emboj.2008.209 Medline

28. P. Fabrizio, B. Laggerbauer, J. Lauber, W. S. Lane, R. Lührmann, An evolutionarily conserved U5 snRNP-specific protein is a GTP-binding factor closely related to the ribosomal translocase EF-2. *EMBO J.* **16**, 4092 (1997). doi:10.1093/emboj/16.13.4092 Medline

29. N. Rasche *et al*., Cwc2 and its human homologue RBM22 promote an active conformation of the spliceosome catalytic centre. *EMBO J.* **31**, 1591 (2012). doi:10.1038/emboj.2011.502 Medline

30. P. Bellare *et al*., A role for ubiquitin in the spliceosome assembly pathway. *Nat. Struct. Mol. Biol.* **15**, 444 (2008). doi:10.1038/nsmb.1401 Medline

31. P. Bellare, A. K. Kutach, A. K. Rines, C. Guthrie, E. J. Sontheimer, Ubiquitin binding by a variant Jab1/MPN domain in the essential pre-mRNA splicing factor Prp8p. *RNA* **12**, 292 (2006). doi:10.1261/rna.2152306 Medline